ChemComm

COMMUNICATION

View Article Online
View Journal | View Issue

Cite this: *Chem. Commun.*, 2023, **59**, 14305

Received 12th September 2023,
Accepted 25th October 2023

DOI: 10.1039/d3cc04519f

rsc.li/chemcomm

Concurrent Cu(II)-initiated Fenton-like reaction and glutathione depletion to escalate chemodynamic therapy†

Ashwini Kumar,‡ Ayushi Chaudhary,‡ Bhumika Agrahari, Kajal Chaudhary, Pooran Kumar and Ritika Gautam Singh *

Chemodynamic therapy is an evolving therapeutic strategy but there are certain limitations associated with its treatment. Herein, we present *de novo* synthesis and mechanistic evaluation of HL1–HL8 ligands and their corresponding $Cu^{II}(L1)_2$–$Cu^{II}(L8)_2$. The most active $Cu(L2)_2$ (IC_{50} = 5.3 μM, MCF-7) complex exclusively depletes glutathione while simultaneously promoting ROS production. $Cu(L2)_2$ also affects other macromolecules like the mitochondrial membrane and DNA while activating the unfolded protein response cascade.

Although cancer treatment has made great strides, it remains one of the leading causes of death.[1] In addition to numerous conventional cancer treatment methods, such as radiotherapy, chemotherapy, and immunotherapy, there have been ongoing efforts to design and develop alternative approaches to overcome the challenges of cancer therapy.[2] In this regard, chemodynamic therapy (CDT) that relies on the principle of ROS generation is an evolving therapeutic strategy due to its high selectivity, minimal adverse effects, and indigenous activation.[3] But there are certain limitations associated with its treatment. The presence of any scavenger could combat the oxidation–reduction equilibrium by quenching the radicals produced.[4] To overcome these limitations, a system that suppresses glutathione while simultaneously promoting reactive oxygen species (ROS) production is required. While a vast majority of compounds that have been discovered for CDT are only capable of targeting one of the two facets of CDT, our proposed molecule is competent at concurrently achieving both aspects.

Herein, we propose a 2-hydroxybenzaldehyde analogue of sirtinol, an inhibitor of Sirtuin protein and their transition metal complexes. Sirtinol and its transition metal complexes with Fe(II), Fe(III), Cu(II), and Zn(II) have been studied for their anticancer properties but their benzaldehyde derivatives have never been explored.[5] Our proposed 2-[(2-hydroxy-1-benzylmethylene)-amino]-*N*-(1-phenylethyl)benzamide molecule is an intriguing scaffold because it can be fragmented down into three distinct units ((a) 2-hydroxy-1-benzylmethylene; (b) 2-iminobenzamide; (c) *N*-1-phenethylamino) that can be independently substituted to produce novel analogues with an increase in the scope and potentially refined activity. As shown in Scheme 1, (*R*, *E*)-2-((2-hydroxybenzylidene)amino)-*N*-(1 phenylethyl)benzamide derivatives **HL1–HL8** were synthesized from (*R*)-2-amino-*N*-(1-phenylethyl)benzamide and 2-hydroxybenzaldehyde with substituted groups at the R^1, R^2, and R^3 positions in EtOH in the presence of catalytic AcOH (Fig. S1–S8, ESI†). Eight corresponding copper(II) complexes **$Cu(L1)_2$–$Cu(L8)_2$** were further synthesized by the reaction of $Cu(OAc)_2{\cdot}H_2O$ with ligands **HL1–HL8**, respectively (Scheme 2, Fig. S9–S16, ESI†). The single crystal for X-Ray diffraction analysis was obtained for **HL2**, **HL3**, **HL4**, **HL5**, **HL8** and **$Cu(L3)_2$**, as shown in Fig. S21 and Tables S1–S4 (ESI†). The resulting crystal structure of **$Cu(L3)_2$** revealed that it exhibited a penta-coordinated trigonal bipyramidal geometry in which the Cu(II) coordination site is conjugated with –ONO atoms of one ligand and –NO atoms of the other ligand from two equivalent **HL3** benzamide Schiff base derivative units. The observed Cu–N bond distances, *i.e.*, 1.974(3) and 1.986(3) Å, and bond angles for O1–Cu1–O3, O1–Cu1–O4 and O3–Cu1–O4 are 151.85(12)°, 98.81(12)° and 108.86(12)°, respectively. These values are consistent with the reported bond angle of trigonal bipyramidal Cu(II) complexes similar to those reported for other iminic donors in trigonal bipyramidal geometries.[6]

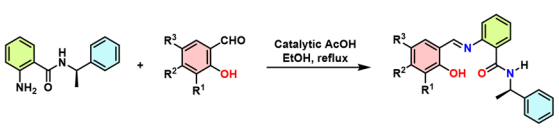

Compounds				Compounds			
HL1	R^1 = H	R^2 = H	R^3 = H	HL5	R^1 = H	R^2 = H	R^3 = F
HL2	R^1 = ^{t}Bu	R^2 = H	R^3 = ^{t}Bu	HL6	R^1 = H	R^2 = H	R^3 = NO_2
HL3	R^1 = H	R^2 = H	R^3 = Cl	HL7	R^1 = H	R^2 = H	R^3 = COOH
HL4	R^1 = H	R^2 = H	R^3 = Br	HL8	R^1 = H	R^2 = $N(Et)_2$	R^3 = H

Scheme 1 Synthesis of the **HL1–HL8** ligands.

Department of Chemistry, Indian Institute of Technology Kanpur, Uttar Pradesh 208016, India. E-mail: rgautam@iitk.ac.in

† Electronic supplementary information (ESI) available. CCDC 2251965–2251969 and 2252221. For ESI and crystallographic data in CIF or other electronic format see DOI: https://doi.org/10.1039/d3cc04519f

‡ These authors contributed equally.

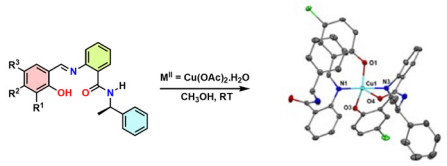

Compounds				Compounds			
$Cu(L1)_2$	R^1 = H	R^2 = H	R^3 = H	$Cu(L5)_2$	R^1 = H	R^2 = H	R^3 = F
$Cu(L2)_2$	R^1 = ^{t}Bu	R^2 = H	R^3 = ^{t}Bu	$Cu(L6)_2$	R^1 = H	R^2 = H	R^3 = NO_2
$Cu(L3)_2$	R^1 = H	R^2 = H	R^3 = Cl	$Cu(L7)_2$	R^1 = H	R^2 = H	R^3 = COOH
$Cu(L4)_2$	R^1 = H	R^2 = H	R^3 = Br	$Cu(L8)_2$	R^1 = H	R^2 = $N(Et)_2$	R^3 = H

Scheme 2 Synthesis of the **Cu(L1)$_2$–Cu(L8)$_2$** complexes.

The stability of **Cu(L1)$_2$–Cu(L8)$_2$** (Fig. S22, ESI†) under simulated physiological conditions (phosphate buffer saline (PBS) solution at pH 7.4 containing 1% DMSO) showed no obvious bathochromic and hypsochromic shift at 0, 1, and 2 h. Our initial screening of (**HL1–HL8**) and **Cu(L1)$_2$–Cu(L8)$_2$** against cancer cell breast adenocarcinoma cell lines MDA-MB-231 and MCF-7, human lung adenocarcinoma cell line A549, human colon cancer cell line HCT-116, and normal human embryonic kidney cell line HEK-293, was determined by resazurin assay, using FDA approved **cisplatin** as the positive control. As demonstrated in Table S8 and Fig. S24–S29 (ESI†), in MDA-MB-231 and MCF-7, the IC_{50} values of the Cu(II) complexes were comparatively higher than those of their corresponding ligands. Our SAR analysis revealed that among Cu(II) complexes, **Cu(L2)$_2$** with *tert*-butyl substitution at the R^1 and R^3 position displayed maximum potency in MCF-7 (IC_{50} = 5.3 μM) comparable to FDA approved **cisplatin**. The cytotoxicity data of **Cu(L2)$_2$** was further confirmed by apoptosis live/dead cell evaluation of MCF-7 by calcein-AM and propidium iodide staining, where **Cu(L2)$_2$** could efficiently induce cell death. While low cytotoxicity was seen in HEK-293 cell lines (IC_{50} = 17.6 μM), **Cu(L2)$_2$** and HL2 incubated erythrocytes at pH 7.4 show considerably low hemolysis even at 200 μM (Fig. S33, ESI†). These data prompted us to venture into the mechanistic understanding of these complexes and **Cu(L2)$_2$** was solicited for further mechanistic studies. We initiated our study by investigating the electrochemical profile of **Cu(L2)$_2$** by cyclic voltammogram (CV). The CV plot of the Cu(II) complex showed a quasi-reversible peak at $E_{1/2}$ = 0.53 V *vs.* Ag/AgCl ($E_{p/a}$ = 0.49 V, $E_{p/c}$ = 0.57 V *vs.* Ag/AgCl) corresponding to the Cu^{II}/Cu^{I} redox couple (Fig. S23, ESI†). The plot for the scan rate effect on the electrochemical behavior of **Cu(L2)$_2$** was found to be linear for both oxidation and reduction events. This further confirms the quasi-reversible redox event. The redox nature and *in vitro* $^{\bullet}$OH radical production ability of **Cu(L2)$_2$** were further confirmed by benzoate hydroxylation and methylene blue degradation assay. Ligands (**HL1–HL8**), once inside the cells can coordinate to the labile Fe(II) and Cu(II) pool and participate in Fenton or Fenton-like chemistry to generate ROS. In benzoate hydroxylation, our results indicate that similar to positive control EDTA, **HL1–HL8** exhibit enhanced levels of salicylate fluorescence intensity and thereby elevated Fenton redox activity of the aqueous Fe(II)/H_2O_2 system (Fig. 1b and Fig. S30, ESI†). The Cu(II) mediated Fenton-like reaction is also evaluated using a colorimetric assay based on the decolorization of FDA-approved methylene blue (MB).[7] The declining absorption spectra of MB at 665 nm (Fig. 1d) showed that the $^{\bullet}$OH radicals were constantly produced once GSH was mixed with MB and **Cu(L2)$_2$** in the presence of H_2O_2. Importantly, no recognizable disappearance of MB was witnessed in the absence of GSH, **Cu(L2)$_2$**, or neither, demonstrating that all three **Cu(L2)$_2$**, H_2O_2, and GSH were essential for generating $^{\bullet}$OH radicals. These $^{\bullet}$OH radicals were successfully trapped and characterized by the EPR technique by utilizing DMPO (5,5-dimethyl-1-pyrroline-*N*-oxide) as a spin trapping agent.[8] The results indicate that upon addition of H_2O_2 and DMPO to the mixture of equimolar **Cu(L2)$_2$** complex and GSH, the 1:2:2:1 quartet signal peak of $^{\bullet}$OH is observed in the EPR spectra. Whereas, when DMPO was added in the presence of only GSH and H_2O_2, there was comparatively low signal peak (Fig. 1c). The *in vitro* observations of $^{\bullet}$OH were implemented in MCF-7 breast carcinoma cells using cell permeable dihydrodichlorofluorescein diacetate (DCFH-DA). Free ligand, **HL2** (2 × IC_{50} and 4 × IC_{50}) and **Cu(L2)$_2$** (2 × IC_{50} and 4 × IC_{50}) show significant bright fluorescent product dichlorofluorescein (Fig. 1e).[9]

With the intent to develop a system that can overcome the limitations of CDT by promoting ROS production while simultaneously depleting glutathione, the interaction of GSH

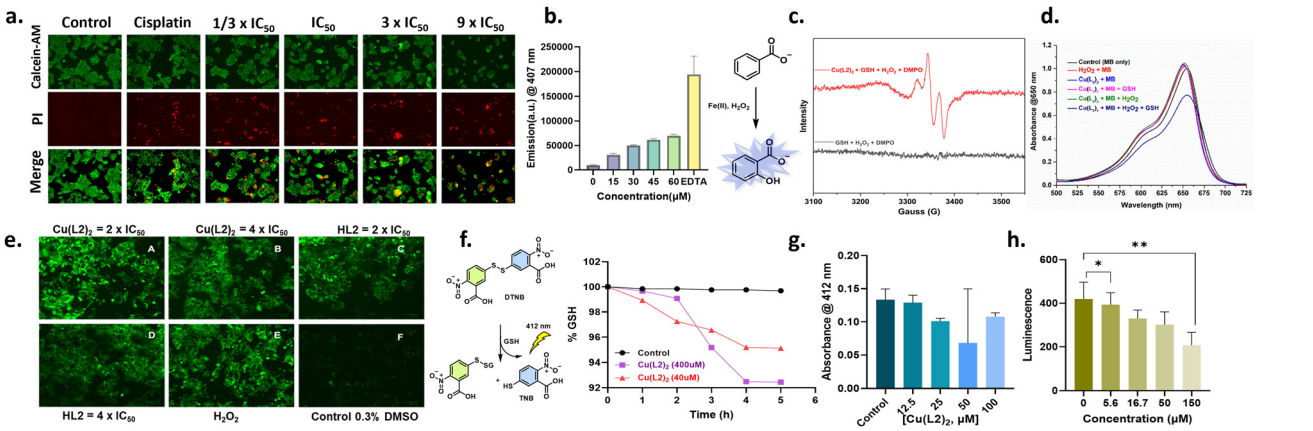

Fig. 1 (a) Live/dead assay (scale bar = 100 μm). (b) Benzoate hydroxylation assay. (c) EPR for radical spin trapping by DMPO. (d) Methylene blue degradation. (e) ROS visualized with DCFH-DA (MCF-7 cells) (scale bar = 100 μm). (f) Decrease in GSH level in MCF-7 cells using Ellman's reagent. (g) Percentage GSH level using Ellman's reagent with **Cu(L2)$_2$**. (h) GSH-Glo™ glutathione luminescence assay (*P < 0.1, **P < 0.01).

with **Cu(L2)$_2$** was investigated by a series of experiments in cell-free as well as in-cell environments. As shown in Fig. S31 (ESI†), ^{1}H NMR spectroscopic study signaled that GSH gets oxidized to GSSG by Cu(II) complexes, while itself getting reduced to a Cu(I) complex. Thus, when **Cu(L2)$_2$** reacted with GSH, the proton signals of **HL2** and the oxidation product GSSG appeared in the ^{1}H NMR spectra. GSH depletion is also verified by quantification with Ellman's reagent, DTNB (5,5′-dithiobis-(2-nitrobenzoic acid).[10] Upon interaction of DTNB with the thiol (–SH) functional group of GSH, a new absorption peak corresponding to 5-thio-2-nitrobenzoic acid appears at 412 nm. As shown in Fig. 1f and g, the intensity of the absorption peak decreased with extended incubation time and increased concentration of the **Cu(L2)$_2$** compared to the initial intense absorption peak at 412 nm. The depletion of GSH was further confirmed using the luminescence-based GSH-Glo™ Glutathione Assay (Promega, USA),[11] where the luciferin derivative gets transformed into luciferin, facilitated by glutathione S-transferase (GST), in the presence of glutathione. Treatment with **Cu(L2)$_2$** led to a significant decrease in luminescence intensity, suggesting a depletion of GSH within the cell. The signal intensity directly correlates with the quantity of unbound GSH currently available within the cellular environment (Fig. 1h).

Free radicals, such as $^{\bullet}$OH and other oxygen-centered related species, have been shown to disrupt a variety of cell macromolecules, including those that make up the electron transport chain, thereby damaging the mitochondrial energy cascade. Using a cell-permeable fluorescent dye containing tetramethylrhodamine methyl ester perchlorate (TMRM), we investigated the mitochondrial membrane potential ($\Delta\Psi_m$) as a gauge for the metabolism, specifically for oxidative phosphorylation leading to ATP production.[12] Following administration of **Cu(L2)$_2$** and **HL2**, a substantial modification in mitochondrial membrane potential was observed, implying depolarization of mitochondrial membrane potential. A higher fluorescence intensity indicates that cells (control) were healthy with intact $\Delta\Psi_m$, but after **Cu(L2)$_2$** and **HL2** treatment, they decreased significantly (Fig. 2a). Simultaneously, a rapid dose dependent depletion of ATP upon treatment with **Cu(L2)$_2$** in the MCF-7 cells (Fig. 2b) was observed, resulting in a 20–40% reduction in ATP levels (Fig. 2b). Without sufficient ATP produced by mitochondria, cancer cells cannot proliferate rapidly. The blockage of macromolecule biosynthesis caused by a lack of ATP due to mitochondrial dysfunction may result in cell cycle arrest. Using propidium iodide (PI) staining and flow cytometry, the impact of **Cu(L2)$_2$** ($2 \times IC_{50}$, $4 \times IC_{50}$, $8 \times IC_{50}$, and control) on the cell cycle was examined. Results from the flow cytometry analysis indicated that compared to the control, the G1 cell cycle phase distribution significantly increases as we increase the concentration of **Cu(L2)$_2$** treatment. This suggests that **Cu(L2)$_2$** treatment inhibits the cellular DNA synthesis and arrests the cells in the G0/G1 phase of the cell cycle (Fig. S35, ESI†).

Overall, GSH functions as a direct antioxidant and a crucial substrate for the GPX4 enzyme to prevent the accumulation of lipid reactive oxygen species; therefore, GSH depletion that ultimately leads to increased lipid peroxidation was monitored by the BODIPY-C11 assay. Oxidation of BODIPY-C11 581/591 was calculated as the ratio of the green (fluorescence emission of the oxidized probe)/red fluorescence mean intensity (fluorescence emission of reduced probe) within the cell outlines. In our study, it was observed that untreated cells did not show any oxidation and thereby no significant accumulation of lipid, while increasing concentration of $10 \times IC_{50}$ and $20 \times IC_{50}$ showed increased oxidized BODIPY-C11, thereby confirming enhanced lipid accumulation (Fig. 2c). Simultaneously, the interaction study of DNA with **Cu(L2)$_2$** by electronic absorption spectroscopy displayed hypochromism in the two absorption bands between 260–290 nm and 400–420 nm, which confirms the interaction with the DNA that can be correlated with the degree of shift (Fig. S32, ESI†). The intrinsic binding constant for the DNA-**Cu(L2)$_2$** complex was determined to be $K_b = (2.2 \pm 0.6) \times 10^5\ M^{-1}$, which is consistent with the previously reported studies.[13]

In addition to affecting a cohort of macromolecules, endoplasmic reticulum (ER) stress is also induced by the accumulation of unfolded protein, hypoxia, or calcium depletion, triggering the unfolded protein response (UPR) cascade.[14] There are three vital UPR pathways that reestablish protein homeostasis in cells: PKR-like ER kinase (PERK), inositol requiring 1 (IRE1), and activating transcription factor 6 (ATF6).[15] Using the western blotting technique, we investigated the concentration-dependent effects of **Cu(L2)$_2$** on PERK markers. As shown in Fig. 2d, at the greatest drug dose of 21.3 μM, for instance, the PERK intensity was approximately 72–75% lower than the control. Direct interaction between PERK and misfolded protein tethers PERK homodimers to initiate oligomerization and ER stress signaling.

Most therapeutics include a cocktail of drugs where combination of different doses with other FDA approved drug helps in accomplishing a greater desired effect with a reduced dosage of each medication, which may further reduce side effects and the likelihood of drug resistance development.[16] The cytotoxicity curve of the corresponding combinations suggests a more potent cytotoxic effect for 1 : 1 and 2 : 1 **cisplatin/Cu(L2)$_2$** but cytotoxicity goes down with 1 : 2 ratio of **cisplatin/Cu(L2)$_2$** (Fig. 2e and Fig. S34, ESI†). The ICP-MS data confirms that the cellular uptake followed the order of **Cu(L2)$_2$** > Cu(OAc)$_2$ > Untreated MCF-7 cells suggesting that the antiproliferative activity of **Cu(L2)$_2$** is concurrent with their lipophilicity and cellular uptake (Fig. 2f).

Of late, there is extensive study being done on the role of bacteria in cancer initiation, proliferation and progression.[17] Cancer patients are highly prone to develop bacterial infection, and this is further made worse by the use of immunosuppressive drugs during cancer treatment.[13] This prompted us to simultaneously investigate the antimicrobial properties of these compounds. The **HL1–HL8**, and **Cu(L1–8)$_2$**, were screened for antimicrobial properties against *S. aureus* (Table S6, ESI†). **HL6**, being exclusively active (MIC of 23.38 μM) can perturb the surface integrity of *S. aureus* ATCC 29213, as examined by atomic force microscopy (AFM) and scanning electron microscopy (SEM). As shown in Fig. 2g and Fig. S36–S39 (ESI†), untreated cells looked bright, smooth, preserved, and had an intact exterior with spherical morphology. However, cells treated for 1 h and 4 h with **HL6** (25, 50 and 100 μM respectively) had a loss of surface morphology and discharge of intracellular content as detritus comparable to complex-treated and 143.1 μM ampicillin-treated cells.

In conclusion, we have successfully established multi-target tumor specific HDAC inhibitor analogues and their Cu(II)

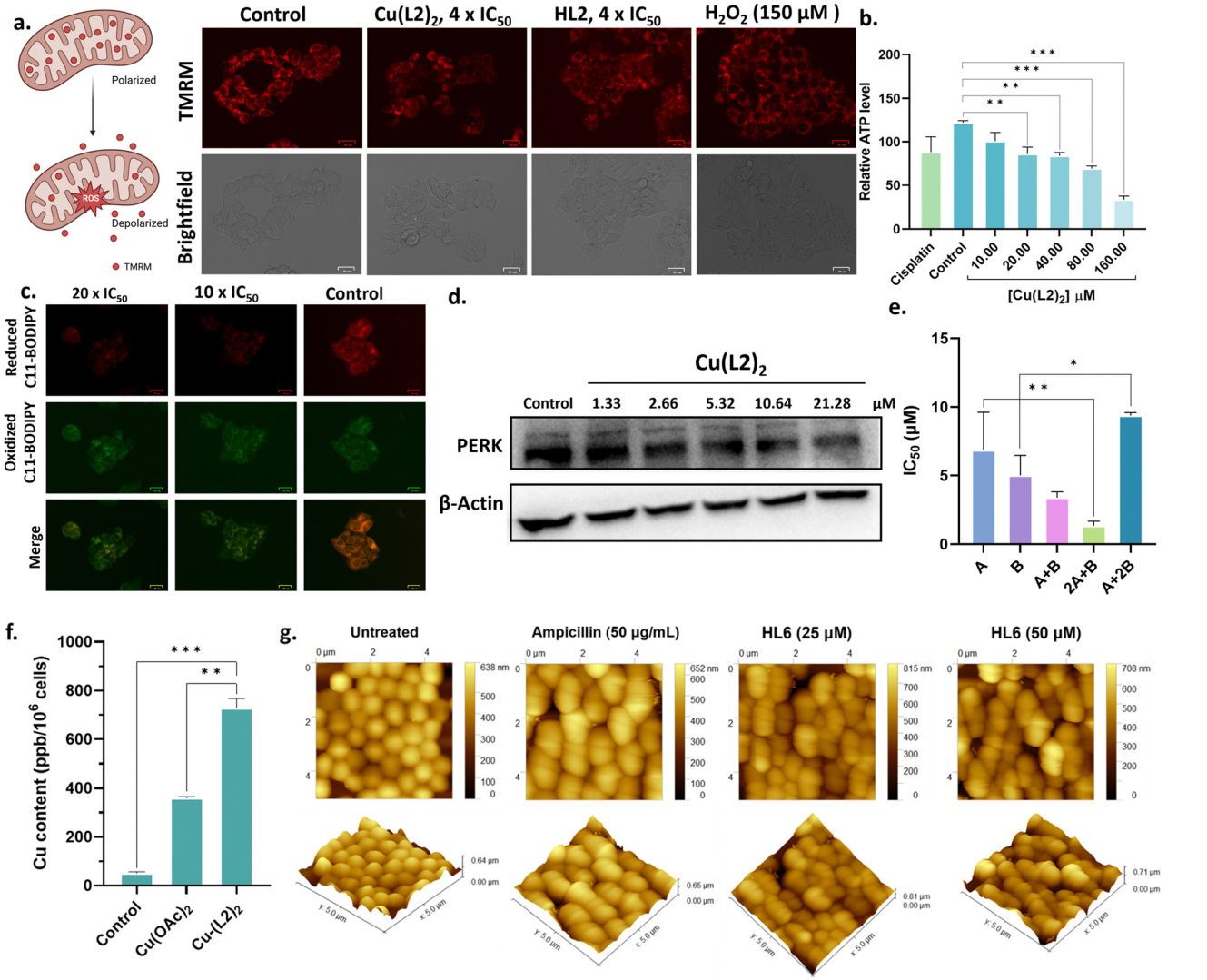

Fig. 2 (a) Mitochondrial membrane potential observed by TMRM dye (scale bar = 25 µm). (b) Decrease of cellular ATP levels, $^{**}P < 0.01$, $^{***}P < 0.0001$ *vs.* control. (c) C11-BODIPY dye–stained MCF-7 cells (scale bar = 25 µm). (d) Western blot analysis of PERK-ER stress biomarkers. (e) The combination analysis of **cisplatin/Cu(L2)$_2$** against MCF-7 cells. (f) Cellular uptake in MCF-7 cells by ICP-MS. (g) AFM 2D topography of *S. aureus* ATCC 29213 cells (left to right) in the absence of and with 143.1 µM ampicillin, and 25 µM and 50 µM **HL6**.

complexes that have the capability to overcome the limitations of CDT by participating in ROS generation while simultaneously targeting multiple sites of action.

This work was supported by the DST SERB Start-up Research Grant (Grant 2021435) and INSPIRE Faculty Research Grant (Grant 2019295), and Prime Minister Research Grant (PMRF-ID: 2300572).

Conflicts of interest

There are no conflicts to declare.

References

1 R. L. Siegel, K. D. Miller, N. S. Wagle and A. Jemal, *Ca-Cancer J. Clin.*, 2023, **73**, 17–48.
2 R. L. Siegel, *et al.*, *Ca-Cancer J. Clin.*, 2019, **69**, 363–385.
3 X. Y. Chen, *et al.*, *Angew. Chem., Int. Ed.*, 2018, **57**, 4902–4906.
4 Z. M. Tang, Y. Y. Liu, M. Y. He and W. B. Bu, *Angew. Chem., Int. Ed.*, 2019, **58**, 946–956.
5 R. Gautam, E. A. Akam, A. V. Astashkin, J. J. Loughrey and E. Tomat, *ChemComm*, 2015, **51**, 5104–5107.
6 L. S. Zheng, *et al.*, *J. Chem. Soc., Dalton Trans.*, 2001, **6**, 845–849.
7 L. L. Li, *et al.*, *J. Am. Chem. Soc.*, 2019, **141**, 849–857.
8 G. R. Buettner, *Free Radic. Res. Commun.*, 1993, **19**, S79–S87.
9 H. Ischiropoulos, *et al.*, *Free Radic. Biol. Med.*, 2012, **52**, 1–6.
10 I. Rahman, A. Kode and S. K. Biswas, *Nat. Protoc.*, 2006, **1**, 3159–3165.
11 A. Pastore, G. Federici, E. Bertini and F. Piemonte, *Clin. Chim. Acta*, 2003, **333**, 19–39.
12 M. D. Brand, *et al.*, *J. Physiol.*, 2012, **590**, 2845–2871.
13 D. Ron and P. Walter, *Nat. Rev. Mol. Cell Biol.*, 2007, **8**, 519–529.
14 P. Walter, *et al.*, *Science*, 2007, **318**, 944–949.
15 K. Dardoufas, *et al.*, *Oral Oncol.*, 2003, **39**, 397–401.
16 G. El Tekle and W. S. Garrett, *Nat. Rev. Cancer*, 2023, **23**, 600–618.
17 D. Mahendiran, S. Amuthakala, N. S. P. Bhuvanesh, R. S. Kumar and A. K. Rahiman, *RSC Adv.*, 2018, **8**, 16973–16990.

